Optimization of Water and Nitrate Use Efficiencies for Almonds Under Micro-Irrigation

Project No.: **11-PREC4-Hopmans**

Project Leader: Jan W Hopmans
Department of Land, and, Air and Water Resources
UC Davis
One Shields Ave.
Davis, CA 95616
530.752.3060
jwhopmans@ucdavis.edu

Project Cooperators and Personnel:
Maziar M. Kandelous, Department of LAWR, UC Davis
Patrick Brown, Department of Plant Science, UC Davis

Objectives:

This field study provides critical information on the movement of water and nutrients through the soil under variable soil moisture conditions, and provides insight into the interactions of applied irrigation water and nitrogen fertilizer, soil physical properties, soil layering and crop root growth with nutrient use efficiency, minimizing losses of water (leaching and evaporation) and nitrogen (leaching and denitrification).

The goal of this research project is to field-validate, optimize and refine the HYDRUS model under a variety of fertigation regimes and two fertilizer sources using the on-going nutrient study in almonds implemented by P. Brown et al. Results will be used to optimize the management of irrigation and fertigation in an almond orchard. The specific objectives of this project are:

1. To evaluate the results of the HYDRUS model using extensive field data for specific treatments, and refine it if so needed;
2. To determine optimal irrigation and fertigation practices for micro-irrigation (drip and micro-sprinkler) systems for almond using HYDRUS, to improve water and nutrient use efficiencies, and to reduce leaching and gaseous losses of nitrates, using a wide range of possible management scenarios (water, fertigation, salinity).

The objectives are achieved by collecting relevant field data such as soil hydraulic and textural properties with soil layering, monitoring of soil moisture and soil water potential, soil temperature and nitrate solution concentration for selected treatments, in addition to data already being collected as part of the larger nutrient management project. A final optimization model will provide best management practices for various relevant micro-irrigation layouts with corresponding optimum irrigation and fertigation scheduling for a range of soil types.

Interpretive Summary:

Micro-irrigation methods have proven to be highly effective in achieving the desired crop yields, but there is increasing evidence suggesting the need for the optimization of irrigation scheduling and management, thereby achieving sustainable agricultural practices, while minimizing losses of applied water and nutrients at the field scale.

To optimize irrigation/fertigation of almonds, it is essential that irrigation and fertilizers are applied at the optimal concentration, place, and time to ensure maximum root uptake. Moreover, sound and sustainable irrigation systems must maintain a long-term salt balance that minimizes both salinity impacts on crop production and salt leaching to the groundwater. The applied irrigation water and dissolved fertilizer, as well as root growth and associated nutrient and water uptake, interact with soil properties and fertilizer source(s) in a complex manner that cannot easily be resolved with 'experience' and field experimentation alone. It is therefore that state-of-the-art modeling is required with the field observations, to allow for unraveling of the most obvious complexities as a result of the typical wide spatial variations of soil texture and layering across farmer-managed fields.

The goal of this research project is to optimize management practices for various micro-irrigation systems for almond, minimizing losses of water (leaching and evaporation), nitrogen (leaching and denitrification), and crop yields by water and salinity stress (droughts). In addition, the applied HYDRUS model with associated root water and nutrient uptake will be evaluated using extensive datasets as acquired from an ongoing nutrient management field project. Therefore, the research project consists of two main components: (a) evaluation of the results of the HYDRUS model using extensive field data for specific treatments, and to refine it if needed, and (b) determining the optimal irrigation and fertigation practices for micro-irrigation (drip and micro-sprinkler) systems for almond using the HYDRUS modeling results, to improve water and nutrient use efficiencies, and to reduce leaching and gaseous losses of nitrates, using a wide range of possible management scenarios (water, fertigation, salinity) and two fertilizer sources.

To achieve this goal this project emphasizes the collection of relevant field data such as soil hydraulic properties, soil texture, and soil layering, and continued monitoring of soil moisture, soil water potential, temperature, salinity, and soil solution nitrate concentration for selected irrigation type treatments. For each of the two irrigation treatments, soil profiles were analyzed to identify soil layers with corresponding textural and hydraulic properties. An extensive set of ECHO-TE soil moisture sensors (Decagon, Inc.), tensiometers, and soil water solution samplers were installed in the tree root zone to monitor the spatial and temporal changes of soil water content, total soil water potential, soil salinity, and temperature. A special tensiometer was designed to monitor and estimate leaching rates of applied irrigation water and nitrate fertilizers.

The 2011-12 annual report focuses on the analysis of field measured soil data, with the ultimate goal to assess and evaluate leaching rates of water across the irrigation season for both irrigation treatments. We tentatively conclude that (a) leaching rates are largely controlled by irrigation type and soil heterogeneity (texture, layering), with irrigation frequency and

applied water being the same, and (b) tensiometers are the critical sensors in monitoring the leaching rate.

Materials and Methods:
The presented methods were used for two micro-irrigation systems, drip and fanjet. For each irrigation system, one tree was selected for detailed instrumentation for the purpose of real-time monitoring of soil- water and tree status. The study is part of an ongoing project at Paramount Farms in Lost Hills (near Bakersfield).

Soil characterization
Among the most important information is an evaluation of the presence of soil layers, and the textural/hydraulic properties of each individual layer for typical soil profiles. Using the layering information obtained from soil cores of last year, we took five undisturbed soil samples (8-cm diameter and 6-cm tall) to measure the hydraulic properties of each identified layer. The constant head method along with multi-step outflow experiment was used to measure the soil water retention curves, saturated hydraulic conductivity, and unsaturated hydraulic conductivity functions for each layer. The multi-step method was introduced by Tuli, et al. (2001), where an initially-saturated soil core is forced to drain by applying a series of positive air pressure steps, while measuring soil core matric potential and drainage outflow volumes during the drainage experiment. The transient outflow and matric potential dataset is used to determine the soil hydraulic properties using a parameter optimization method. Also, the bulk density, porosity, saturated water content, and the soil texture of each individual core was determined.

Soil monitoring

Soil moisture and soil water potential
Unfortunately, many of ECHO-5TE (Decagon Inc) soil moisture sensors installed by PureSense last year were broken because of malfunctioning of sensors and data collection issues. Therefore, we planned for a new installation set-up with collaboration of PureSense Environmental Inc. A total of 30 ECHO-5TE (Decagon Inc) soil moisture sensors were installed in the rooting zone of each of the two tree locations in a grid pattern (**Figure 1**), thereby instrumenting one quarter of the tree's rooting zone, at depths of 30, 60, 90, 120 and 150 cm for 6 spatial locations (**Figure 2**). An additional set of sensors installed at the same depths below the berm was installed in the fanjet plot along the center line (Y-direction) (**Figure 2**). The sensor installation grid is designed such that measurements provide soil information halfway between trees (Y direction), and up to the distance influenced by wetting pattern of either fanjet or drip perpendicular to the trees row (in X direction).

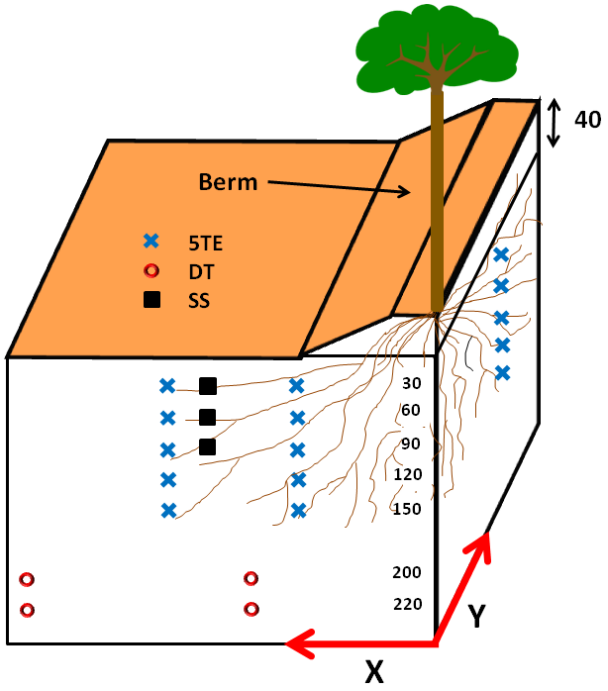

Figure 1. A schematic showing installation depths of various sensor types, with 5TE representing the ECHO-5TE soil moisture, DT the deep tensiometers, and SS referring to soil solution samplers

The ECHO-5TE provides for measurement of

volumetric soil water content, as well as for soil salinity (Electrical Conductivity or EC), and soil temperature. For the purpose of installation, holes were dug with a 5" hand auger. Sensors were provided and are being monitored by PureSense Environmental Inc.

Four pairs of deep tensiometers (red circles) were installed at both fanjet and drip irrigation sites to monitor the total head gradient below the root zone. Two pairs of tensiometers were installed below the canopy where the irrigation water is applied representing the wet part of the root zone and the other two pairs were placed at the middle distance between two trees' rows representing the driest spot of the root zone.

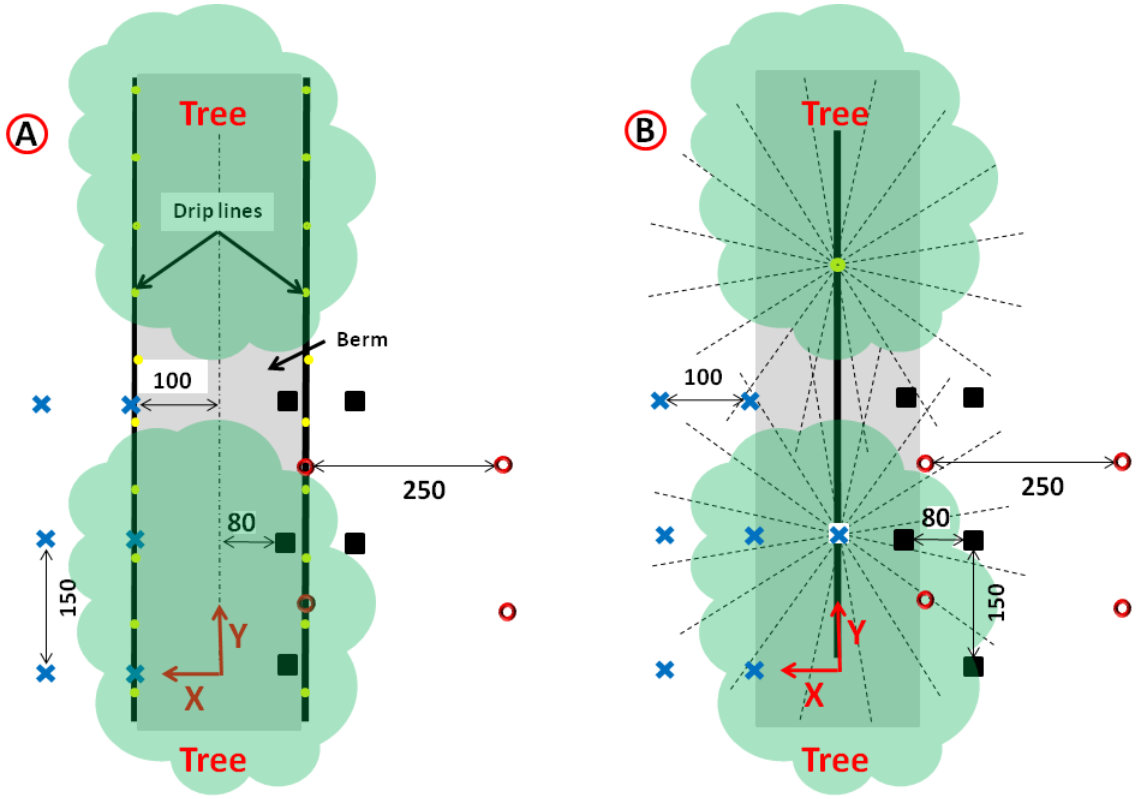

Figure 2. A schematic top view of the installed soil moisture sensors, deep tensiometers, and solution samplers in (A) Drip and (B) Fanjet site.

Leaching rate calculations

Leaching rates can be measured if the hydraulic conductivity and the total head gradient across the soil layer below the root zone are known. The leaching flow rate, q_{AB}, can be calculated using the Darcy equation as follows:

$$q_{AB} = -K(h)\frac{H_B - H_A}{\Delta z_{A-B}} \quad , \qquad (1)$$

where *q* denotes the Darcy water flux (cm day $^{-1}$), *K(h)* represent the unsaturated soil hydraulic conductivity, which is a function of the soil matric potential *h* at the measurement depth. In the Darcy equation, H_A and H_B denote the total water head values at bottom and top of the soil layer below the root zone, respectively, and Δz_{A-B} signifies the thickness of the soillayer between the tensiometers. As was shown in **Figure 1** the set of deep tensiometers were installed at four different locations at depths of 200 and 220 cm. Using the measured soil matric potential values above and below the impeding layer and its thickness, we computed the total head gradient of each of four individual locations for each site. Using the measured soil water matric potentials along with the unsaturated hydraulic conductivity curve (**Figure 7**) for the soil layer at each location, leaching rates were calculated by multiplying the unsaturated hydraulic conductivity with the total head gradient according to Eq. [1].

Deep tensiometer design

Leaching rates require continuous head gradient measurements across the soil layer of interest below the rooting zone. However, the vertical tensiometer length is one of the main factors limiting its operation range. To remove this constraint for deeper soil water tensiometric measurements, we developed a special deep tensiometer that can be operated across the maximum application range (0- 850 cm). This was done by installing the pressure transducer at the tensiometer cup, as opposed to conventional tensiometers where the pressure transducer is installed at the soil surface, using a hanging water column. **Figure 3b** shows the result of laboratory evaluation of the new design for several wetting and drying cycles, including times at which the tensiometer was serviced by refilling with water (blue arrows). The component of this new designed tensiometer is presented in **Figure 3a**.

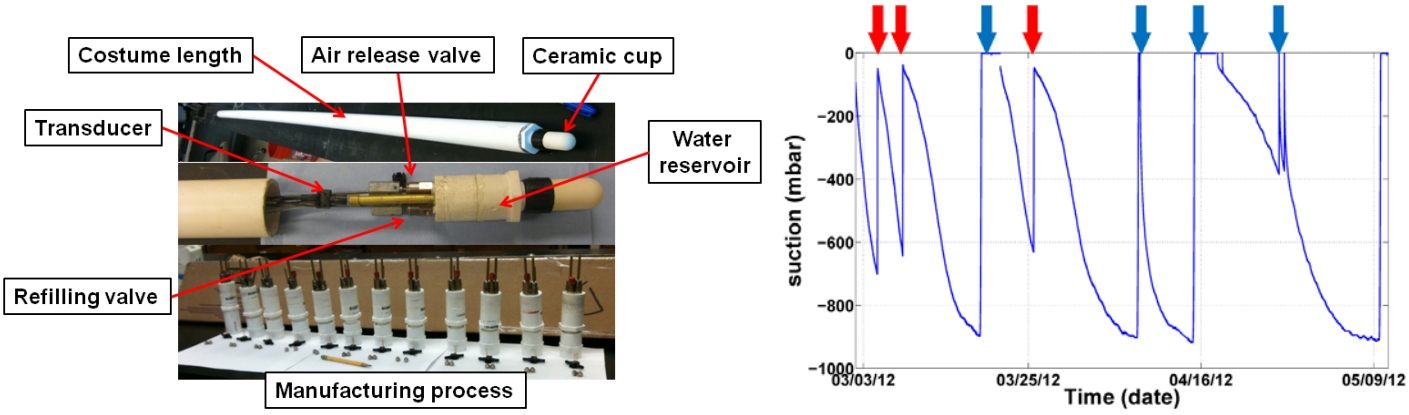

Figure 3. (a) Deep tensiometer design and (b) Laboratory evaluation of the deep tensiometer during wetting and drying cycles. Red arrows show soil wetting with blue arrows representing times of refilling the tensiometer cup.

We believe this new design is critical for application in irrigated systems requiring tensiometer measurements at large depths below the rooting zone, to estimate soil water leaching rates.

Additional required input data for modeling

In addition to soil physical characterization, other required input data for the HYDRUS modeling includes measurements of tree evapotranspiration (ET), water application rates and spatial distribution for the drip and fanjet systems, fertigation amounts and rates, and tree root distribution. Daily ET rates are available from eddy-covariance data collected at the fanjet site, whereas volumetric flow rates are determined from flow meter measurements installed in the irrigation lines. The wetted area for the drip system is monitored by visual inspection, whereas the water application uniformity of the fanjet system was determined from measurement of water volumes in 110 10-cm diameter catch cans, distributed within the quarter section of the instrumented fan jet plot (**Figure. 4**). Though additional uniformity data will be collected, soil moisture patterns indicate that the measured patterns are consistent during the irrigation season. During the 2012 irrigation season, soil solution nitrate samples were collected during and between three fertigations and patterns are evident, however, additional nitrate data will have to be collected and analyzed.

Figure 4. Measurement (a and b) of water application uniformity and uniformity pattern (c) for the fan jet (1 hour volume measurements).

Results and Discussion:

Soil textural analysis and hydraulic properties

The analysis of soil texture for both the fanjet and drip sites showed that the soil profile of the studied almond orchard is highly heterogeneous and layered. **Figure 4** shows representative soil layers and differences of soil profiles between the drip and fanjet site. The top one meter of soil profile at the fanjet site consists of coarse soil material, allowing quick infiltration of applied irrigation water. The profile includes two 20 cm thick fine-textured soil layers at approximate depths of 130 and 200 cm. These layers will prevent and/or delay downward water movement below the root zone. The drip site shows depth variations in soil texture as well, with the fine-textured soil layer at about the 180 cm soil depth. We believe the difference in depths of clay layers between the two irrigation plots has significant implications on leaching rates.

Fan Jet	Clay (%)	Silt (%)	Sand (%)	Depth (cm)	Sand (%)	Silt (%)	Clay (%)	Drip
Sandy clay loam	21	18	61	10	73	12	15	Sandy loam
				20				
				30				
	27	26	47	40	75	13	12	
				50				
				60				
	21	26	53	70	72	15	13	
				80				
				90				
Loam	28	27	45	100				
				110	37	32	31	Clay loam
				120				
Clay	54	27	19	130	43	38	19	loam
				140				
Sandy loam	19	25	56	150				
				160	48	27	25	Sandy clay loam
loam	23	32	45	170				
Sandy loam	14	12	74	180				
				190	21	37	42	Clay
Silt clay	44	47	6	200				
				210				
Clay loam	29	37	34	220	37	29	34	Clay loam
				230				
				240				
				250	62	19	19	Sandy loam
				260				
				270				

Figure 5. A schematic with soil layers and soil texture for the drip and fanjet sites.

A total of five core samples (8-cm diameter and 6-cm tall) were

collected from each of the main soil layers in the drip site, for the purpose to measure their soil water retention and unsaturated hydraulic conductivity curves, together with soil bulk density, saturated water content, and soil texture (**Figure 6**). Although the combined data in **Figure 6** are generally consistent, as saturated hydraulic conductivity increase with saturated water content, and lower dry soil density, the depth variation of soil texture is very different from the 2011 depth distribution of soil textural layers (**Figure 5**). In general, we conclude that depth variation of soil textural layers is enormous at the tree plot scale, thus introducing large uncertainty in specific soil layering depths. **Figure 7** shows the soil water retention and unsaturated hydraulic conductivity curves for the five core sample from different soil textural layers. However, further soil core sampling at both experimental sites is needed to ascertain the depth variation of soil texture and hydraulic properties, and their spatial heterogeneity of soil profiles within and between the two irrigation sites.

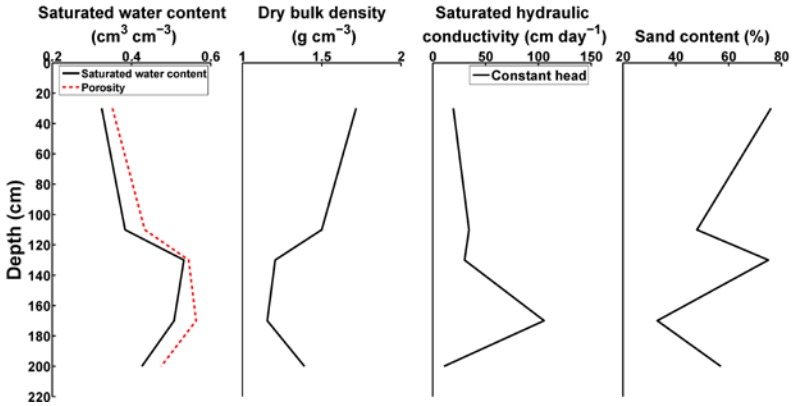

Figure 6. Saturated water content, dry bulk density, saturated hydraulic conductivity, and sand content as a function of depth for the drip site.

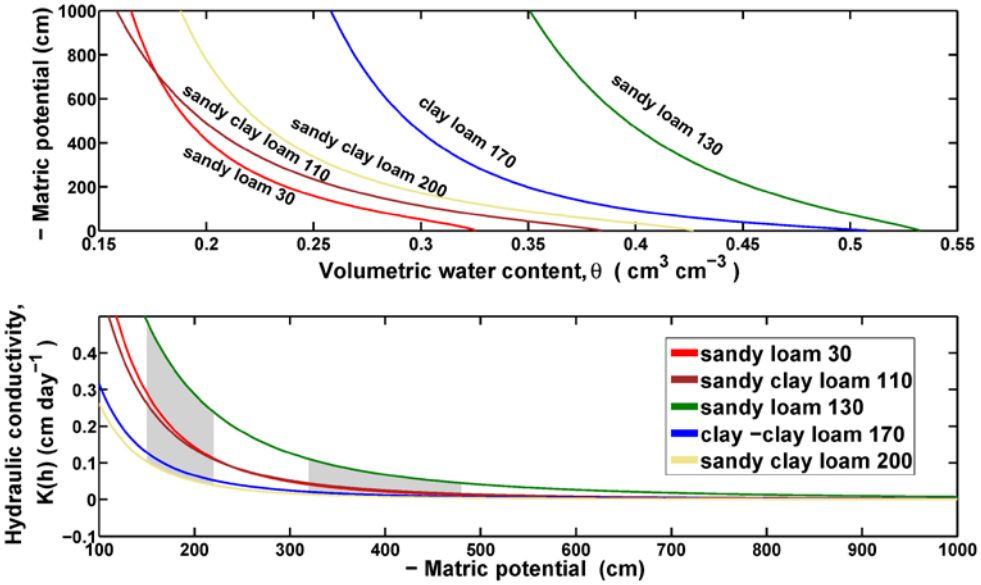

Figure 7. Soil water retention and unsaturated hydraulic conductivity curves for the different soil types. Shaded portions represent the variation in unsaturated hydraulic values as a result of variations in measured soil water pressure head values across the field plot sites.

Soil moisture measurements

Figures 8 and 9 present the spatial and temporal variation of soil water content in the root zone for the drip and fanjet irrigation site under new installation setup, respectively. The pink and blue bars indicate the irrigation and rain events during the presented time period, respectively. The (X, Y) notation represents the Cartesian coordinate system, with both X and Y, representing distances (cm) from the tree trunk. For example, the panel with the (0,150) notation presents soil water content data that is exactly along the tree row (X = 0 cm) and midway between the trees (Y = 150). Similar to the previous year data set, the sensors installed at depths of 30 and 60 (and 90 cm added this year) in the drip site (**Figure 8**) respond to the irrigation and precipitation events showing the affected soil profile by the moving wetting front. The mild response of Echo sensors at the 120 and 150 cm soil depth along with their relatively high and constant water content values is a reflection of the perching of water above the 180 cm depth clay layer (**Figure 5**), with the depth variation above 120 cm caused by variable-textured soil layers.

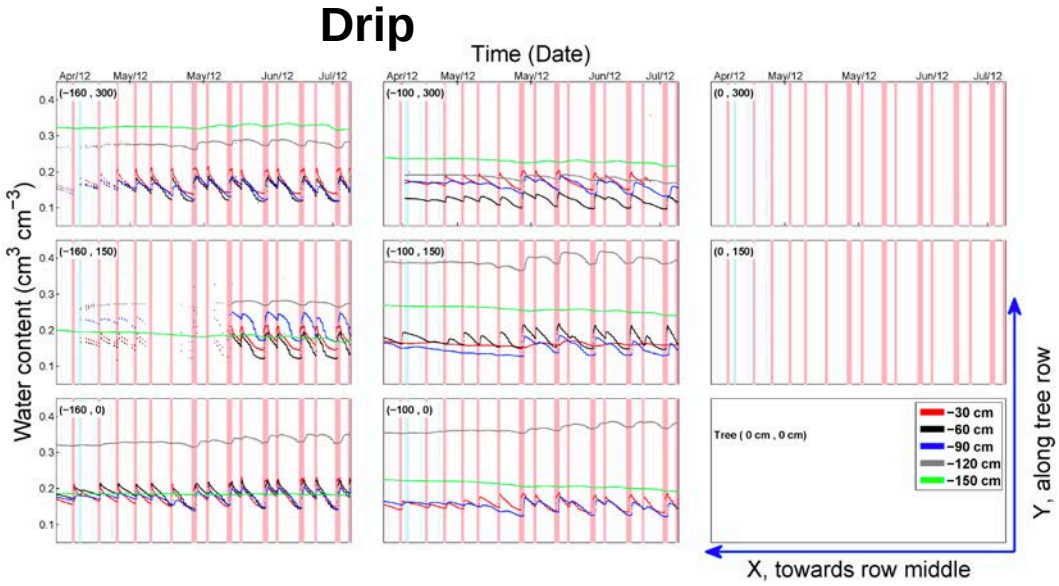

Figure 8. Spatial and temporal variations of soil water content in the root zone under **drip** irrigation system. The pink bars indicate the irrigation events and the blue bars denote the precipitation events. The width of each bar represent the duration of each irrigation or precipitation events.

For the fanjet soil moisture measurements of **Figure 9**, the shallow sensors at depths of 30 and 60 cm immediately respond to the irrigation event, but to a lesser extent than for the drip irrigation. The presence of the clay layer at the 120 soil depth (**Figure 5**) causes water to perch, which leads to the highest water content values across the fanjet plot. The lower water content at the 150 cm soil depth can be explained by reduced leaching across the clay layer, with spatial variations caused by nonuniform water application pattern and soil heterogeneities. In fact, spatial variations in root zone water content can be related to the water application pattern of **Figure 4**.

Though we have confidence in the measured temporal soil moisture trends, additional moisture sensor calibration is required to assess the uncertainty of absolute soil moisture values.

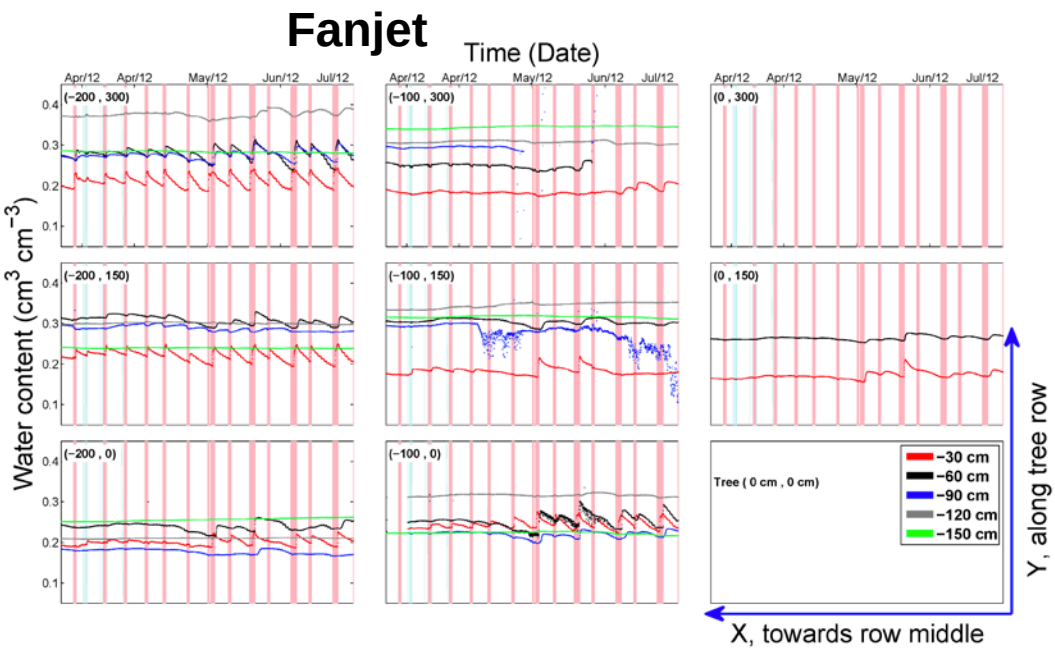

Figure 9. Spatial and temporal variations of soil water content in the root zone under **fanjet** irrigation system. The pink bars indicate the irrigation events and the blue bars denote the precipitation events. The width of each bar represent the duration of each irrigation or precipitation events.

Leaching rates

Leaching rates were computed from the Darcy Eq. [1], considering the uncertainty in (a) soil water matric potential measurements, (b) unsaturated hydraulic conductivity curves, and (c) soil texture of the soil layers of the tensiometer locations. Therefore, rather than calculating single leaching rate values, we computed leaching rate uncertainty.

Figures 10a and **11a** present the average, minimum, and maximum matric potential values measured at both the 200 and 220 cm soil depths for the drip and fanjet sites, respectively. As a result of increasing root water uptake and crop transpiration from spring to summer, the matric potential of the soil layer below the root zone gradually decreases (more negative) for both irrigation sites. We note that the matric potential values of the drip site are much larger (less negative) than for the fanjet site, because of the clay layer presence at the tensiometer depth. The drier soil at the fanjet site is caused by reduced redistribution from the existing clay layer at the 120 cm depth (**Figure 5**). The much larger uncertainty of the matric head values at the fanjet location is likely caused by the nonuniformity of the water application and reduced lateral spreading, as opposed to the drip site with higher water content values above the deep clay layer.

From the measured matric head values at the 200 and 220 cm soil depths, the total head gradient with corresponding spatial variations (min and max values) are plotted in **Figures 10b and 11b**. Typically, average total head gradients vary between 2 and 4, indicating downward soil water flow, but decrease through the summer to between 0 and 2. Some locations show negative total head gradients in the mid to late summer, resulting in upwards capillary flow into the tree root zone. Variations are typically large, and are caused by uncertainty in tensiometer readings and soil heterogeneity.

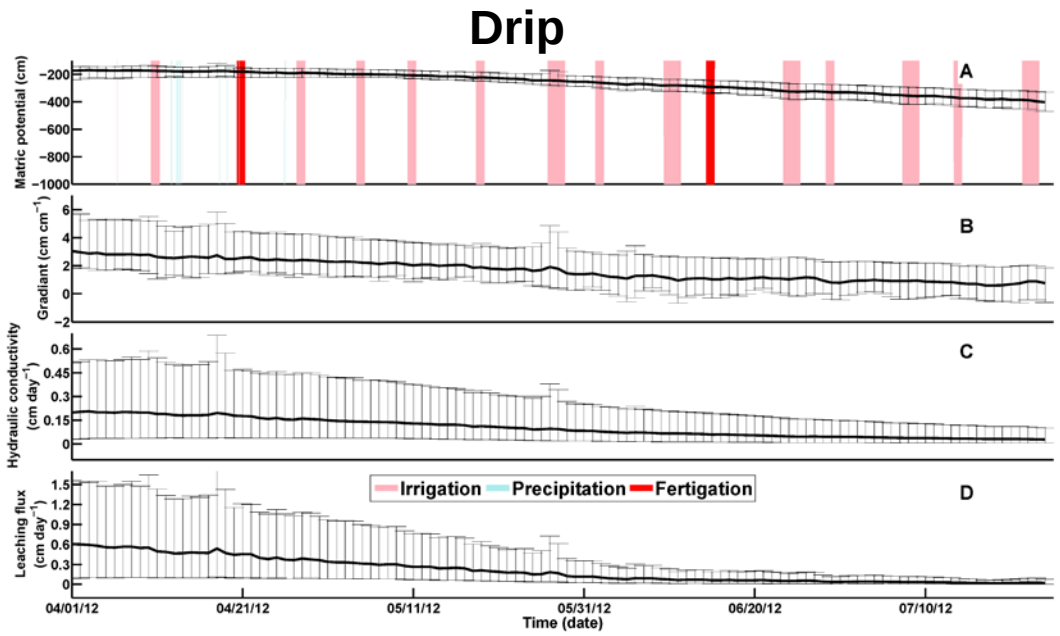

Figure 10. Spatial variations of (a) matric potential at the 200 and 200 cm soil depth, (b) total head gradient, (c) unsaturated hydraulic conductivity, and (d) leaching rate for the **drip** system, as measured for 4 locations (**Figure 1**), starting April 1 through July 27. Average values are presented by the thick black lines, whereas the spatial variations are presented by the error bars, defined by corresponding minimum and maximum values (error bars). The pink, blue, and red bars represent irrigation, precipitation, and fertigation events, respectively.

In order to compute the leaching rate at the 200-220 cm soil depth, we need to substitute the unsaturated hydraulic conductivity value of this layer in Eq. [1], which is dependent on the soil texture and soil water matric potential (**Figure 7b**) at the tensiometer locations. However, because of the large variations in both matric potential and soil texture, we present the range in unsaturated hydraulic conductivity (**Figure. 10c and 11c**) as determined from the uncertainty ranges of matric potential (**Figure 10a and 11a**) and unsaturated hydraulic conductivity curves (**Figure 7**). The latter is controlled by soil texture, but is partly unknown because of the apparent high spatial variability of soil texture and soil layering. Therefore, we calculated the unsaturated hydraulic conductivity of all the soil types for the given range of matric potential as presented by the filled-in areas in **Figure 7.** The much higher unsaturated hydraulic conductivity values for the drip site are a result of the higher soil water matric potential (compare **Figure 10a** with **Figure 11a**) at the 200 cm depth. Despite the large variation in matric potential for the fanjet, the corresponding uncertainty range for the hydraulic conductivity is smaller than for the drip site, and is a result of the much lower matric potential (more negative) for the fanjet site. The final estimated leaching rate values are presented in **Figures 10d** and **11d**, showing that both the average and variation of the leaching rates is much higher for the drip site than for the fanjet site, with mean leaching rate values ranging between 0-6 mm/day (drip) and 0-1 mm/day for the fanjet. We hypothesize that the much lower leaching rates for the fanjet site is mainly caused by the impeding clay layer at the 120 cm depth. However, additional soil core sampling is required to reduce the uncertainty of the hydraulic characterization at the 200 depth.

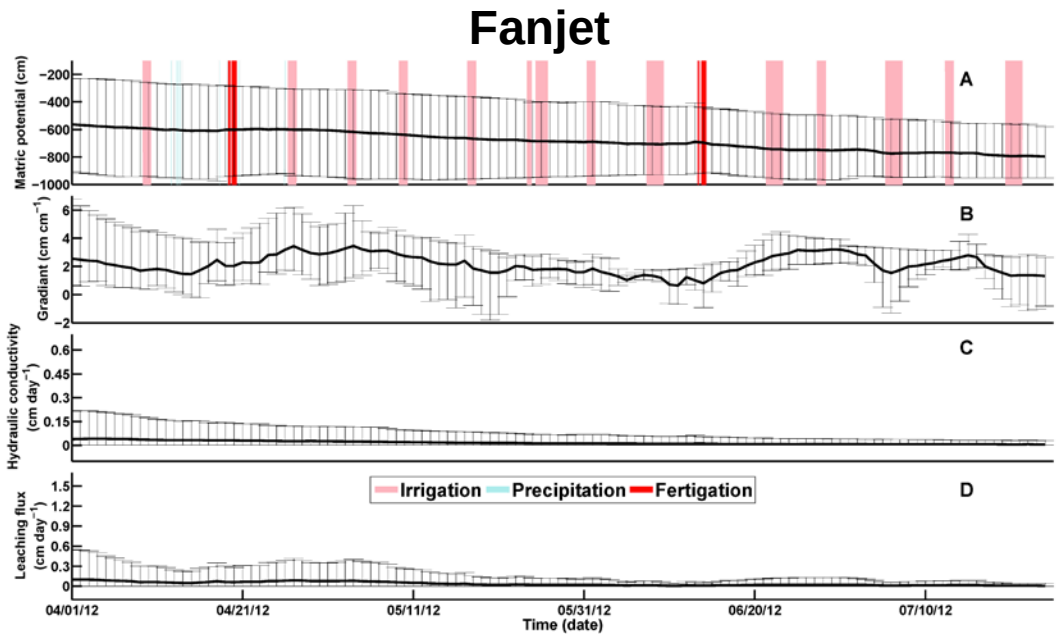

Figure 11. Spatial variations of (a) matric potential at the 200 and 200 cm soil depth, (b) total head gradient, (c) unsaturated hydraulic conductivity, and (d) leaching rate for the **fanjet** system, as measured for 4 locations (**Figure 1**), starting April 1 through July 27. Average values are presented by the thick black lines, whereas the spatial variations are presented by the error bars, defined by corresponding minimum and maximum values (error bars). The pink, blue, and red bars represent irrigation, precipitation, and fertigation events, respectively.

Soil electrical conductivity

Figure 12 shows the temporal variations of soil electrical conductivity (EC) at different depths in both fanjet and drip sites, as determined by Blake Sanden. These soil salinity data confirm our hypothesis that the leaching rates are controlled by the most shallow clay layer within the soil profile (as represented by the gray bands in **Figure 12**). The lower leaching rates cause higher soil salinity in the soil profile of the fanjet site.

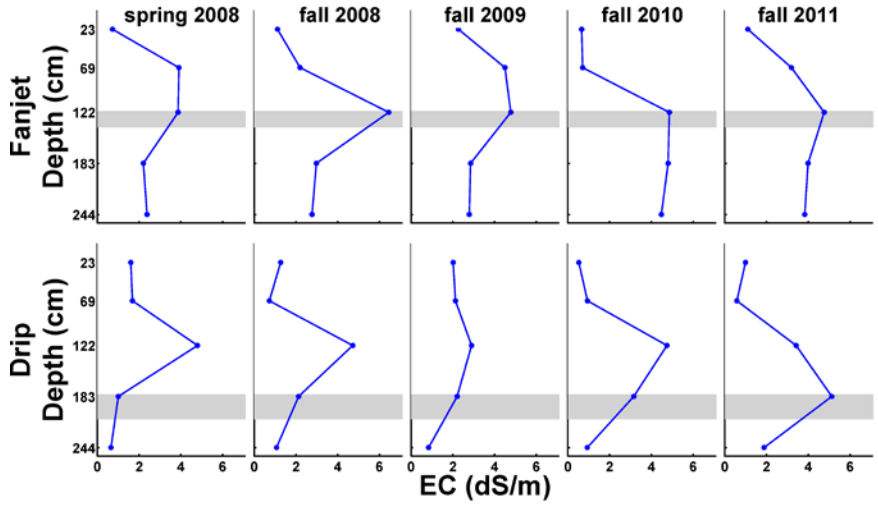

Figure 12. Temporal variations of soil electrical conductivity (EC) at different depth in both fanjet and drip sites. The horizontal gray bar represents the clay layer. Data provided by Blake Sanden.

Research Effort Recent Publications:

Hopmans, J.W., M.M. Kandelous, A. Olivos, B.R. Hanson and P. Brown. 2010. Optimization of water use and nitrate use for almonds under micro-irrigation. Almond Industry Conference, Modesto, CA.

Kandelous, M.M, T. Kamai, J.A. Vrugt, J. Simunek, B.R. Hanson and J.W. Hopmans. 2010. An optimization model to design and manage subsurface drip irrigation system for alfalfa. AGU Fall meeting, San Francisco, CA.

Kandelous, M.M, A. Olivos, P. Brown, and J.W. Hopmans, 2011. Optimization of water use and nitrate use for almonds under micro-irrigation. Almond Industry Conference, Modesto, CA.

References Cited:

Tuli, A., M. A. Denton, J. W. Hopmans, T. Harter, and J. L. Mac Intyre. 2001. Multi-step outflow experiment: From soil preparation to parameter estimation. LAWR Rep. 100037 (http://researchers.lawr.ucdavis.edu/tuli/REPRINTS/MULTISTEPOUTFLOW.pdf)